Batch-Screening Guided Continuous Flow Synthesis of the Metal-organic Framework HKUST-1 in a Millifluidic Droplet Reactor

Rajasi Shukre[1], Thomas Ericson[2], Daniel Unruh[2], Hannah Harbin[1], Anthony Cozzolino[2], Chau-Chyun Chen[1], and Siva Vanapalli*[1]

[1] *Department of Chemical Engineering, Texas Tech University, Lubbock, Texas -79409*
[2] *Department of Chemistry and Biochemistry, Texas Tech University, Lubbock, Texas -79409*

ABSTRACT

Metal-organic frameworks (MOFs) are a class of crystalline and porous adsorbents, with wide-ranging applications in gas separations, membrane materials as well as sensors. Commonly used batch synthesis techniques for MOF production are limited by low productivity, high operating costs, and slow crystallization timescales, severely impeding the large-scale manufacturing of these materials. However, batch synthesis is a useful and easy technique to screen multiple reaction parameters to find an optimal chemistry. Therefore, in this study, we have used the batch process and screened a multidimensional reaction space consisting of 45 sample variations based on the crystallinity, yield and instantaneous precipitation, which could lead to tube clogging under flow conditions. We have found one optimized reaction chemistry, that could be used in flow conditions, which in this study is a novel millifluidic droplet-based reactor for the continuous synthesis of HKUST-1 crystals. The biphasic flow in the millifluidic reactor consisted of droplets of the reactant solution, dispersed in a continuous phase of silicone oil. We investigate the differences in the quality and quantity of HKUST-1 synthesized via the continuous and batch techniques. Moreover, we have demonstrated that the HKUST-1 samples prepared via the continuous synthesis in a droplet based millifluidic reactor, at an ultra-low residence time exhibit excellent physical properties comparable to that obtained for the samples prepared by the traditional batch process. A clean, easy-to-install, and reusable millifluidic reactor presented in this work may pave the path for an economically viable, large-scale synthesis of HKUST-1.

1. INTRODUCTION

Metal-organic frameworks (MOFs) are porous crystalline solids containing organic linker molecules and inorganic secondary building units. The linker molecules are unsaturated hydrocarbons, mostly containing benzene rings with multiple binding groups such as carboxylic acids. The deprotonated carboxylate binding groups coordinate with metal ions in solution to form polynuclear clusters called the secondary building units [1]. The self-assembly of such units ultimately leads to the formation of crystalline frameworks with ultrahigh porosities and surface area, in comparison to the typical adsorbents such as activated carbon and zeolites [2]. The pore volume and surface area of these materials can be synthetically tuned to generate isoreticular frameworks for desired applications [2]. These materials exhibit high structural stability even after post-synthetic modification, wherein adsorption and catalytic sites are created in addition to the enhancement of hydrothermal stability [3, 4]. Thus, with many beneficial properties, MOFs potentially have a diverse portfolio of applications in catalysis [2–5], chemical sensors [6], carbon capture [7], water harvesting from the atmosphere [8–10], removal of heavy metals from water [11] and capture of toxic chemicals [12].

Traditionally, batch processes have been used for MOF synthesis, with large residence times ranging from hours to days [13]. The solvothermal technique is the standard procedure for MOF synthesis wherein the reaction between the metal-salt and the organic linker occurs in the solution phase at elevated temperature and autogenous pressure conditions within a sealed autoclave. Batch techniques can have drawbacks associated with slow crystallization times, low mixing efficiency, poor yield and

*Corresponding Author: siva.vanapalli@ttu.edu (✉)

Table 1: **Summary of previous microfluidic approaches for MOF synthesis.** (**T** is temperature, $\mathbf{t}_r$ is the residence time, **P** is the pressure, $\mathbf{S}_{BET}$ is the BET surface area of MOF, $\mathbf{d}_p$ is particle size of MOF crystal.)

Authors	**MOF**	**Heating element**	**T** (°C)	$\mathbf{t}_r$ (mins)	**P** (bar)	**Yield**	$\mathbf{S}_{BET}$ (m^2/g)	$\mathbf{d}_p$ (μm)
Faustini et al. [39]	HKUST-1	Heated Oil bath	90	1-12	1	5-68%	600-1911	5-15
Faustini et al. [39]	IRMOF-3	Heated Oil bath	120	3	1	---	2428	10-15
Faustini et al. [39]	MOF-5	Heated Oil bath	120	3	1	---	3185	10-15
Faustini et al. [39]	UiO-66	Heated Oil bath	140	15	1	---	1095	10-15
Paseta et al. [40]	Fe-MIL -88B-NH_2	Heated Oil bath	55-95	0.33-10	1	0.6-12.4%	---	0.18-0.9
Jambovane et al. [41]	UiO-66 -NH_2	Oven	120	60	1	5 mg/hr	910	0.08-0.1
Bagi et al. [14]	Ni_2Cl_2 (BTDD)	Al tubes and blocks	140	60	6.8	80%	2157	---
Bagi et al. [42]	MOF-808	Al tubes and blocks	150	5	4	80%	1600	0.14
This work	HKUST-1	Al Block	80	13	1	15%	1615	14.5±11.6

copious amounts of solvent usage potentially increasing the cost of the final product [14]. Addressing these drawbacks, several innovative techniques such as microwave-assisted heating [15–19], ultrasound [20,21], electrochemical [22,23] and mechanochemical synthesis [24] have been demonstrated to overcome the limitation of long residence times in conventional batch reactors. Nevertheless, the non-conventional approaches can be severely limiting due to the high capital and operating costs [25–27], poor crystallinity of the MOFs [20] and reduced surface area due to clogging of the pores of the resultant frameworks [23,24].

Contrasting batch reactor approaches, continuous flow reactors offer high productivity, high space-time yields, and are operable in various configurations [28–31]. Nevertheless, the use of these reactors is associated with high operating cost, low surface area to volume ratio, poor mixing, and particle clogging. In one of the configurations, counter-current mixing of reactants with a high-temperature water jet led to rapid crystallization and high surface area, but nonetheless rendered high operating costs [32]. In another configuration, a draft-tube baffled reactor with recycle stream provided high productivity but was limited by particle agglomeration leading to clogged outlet stream [33]. Moreover, a high space time yield was obtained with high feed concentration of reactants in a continuous stirred tank reactor, but the surface area of the MOF was drastically reduced due to inter-penetrated structure [34]. In tubular reactors with diameters in the millifluidic range, complete crystallization was observed within a few minutes with high yield ($\geq$ 85%) and surface area [35–38]. Nevertheless, the quantity and quality of the MOFs improved with an increase in the temperature, which necessitated application of high back pressure (20-250 bar) to maintain the liquid phase in the reactor [35–37], leading to high operational costs.

Microfluidic and millifluidic two-phase reactors circumvent the limitations of continuous flow reactors [14,39–45]. A summary of various MOFs synthesized using the micro/millifluidic techniques is presented in Table 1. In these reactors, droplets of the reaction mixture co-flow with a continuous oil phase in a narrow channel. Each droplet constitutes an independent reactor with high surface area to

volume ratio where chaotic advection currents not only accelerate the crystallization but also provide fine tuning of the particle size [45–47]. Different MOFs have been synthesized via this technique with reaction times in minutes [39]. A narrow range of particle size distribution of a MOF was obtained by controlling the droplet volume and the residence time [40]. In another work, simultaneous synthesis and functionalization of a particular MOF was performed within an hour [41]. These droplet-based reactors produced high yield with potential parallelization [14], increased the throughput and reduced the solvent usage [42].

Despite the attractiveness of droplet-based micro/millifluidic reactors, the following challenges still exist: (i) Depending on the reagents used for MOF synthesis, the reaction rates might be fast or comparable to the timescales for producing droplets, leading to the clogging of the droplet generators. Thus, an optimal reaction chemistry must be chosen so that the continuous flow synthesis can proceed without interruption, (ii) the flow conditions need to be optimized to optimize the timescale of droplet production, droplet volumes, and residence times, and (iii) due to the continuous flow, the temperature and heating elements need to be optimized to ensure efficient heat transfer. Otherwise, vapor bubbles can form that can disrupt the continuous flow synthesis.

In this study, we address these challenges by taking a batch screening approach that allows us to identify MOF reaction parameters that are suitable for implementation in a millifluidic droplet reactor for continuous synthesis. The advantage of this approach is that batch screening allows rapid assessment of the reaction parameters without the need to additionally optimize multiple flow parameters that would be required if done by only continuous synthesis. To the best of our knowledge, such a batch-guided screening process of the reaction space has not been performed in prior continuous flow synthesis of MOFs. In addition, we implement, visual monitoring of the reaction in the millifluidic droplet reactor, to examine stability of the two-phase flow and color of the product particles which can assist in identifying flow rates, temperature and reaction parameters that are optimal.

For our study, we have chosen to synthesize HKUST-1 (Cu_3BTC_2) because it is one of the best adsorbents for natural gas and hydrogen storage [1]. This MOF owes its adsorbing properties to the high BET surface area in the range of 1200-1800 m^2/g [48], an overall void space of 40.7%, and the presence of open metal sites [1]. We have performed extensive experimentation using batch process to screen a multidimensional reaction space, to obtain an optimum set of parameters suitable for the millifluidic synthesis. Moreover, we have performed a thorough characterization of HKUST-1 synthesized via this millifluidic reactor and compared the properties in detail with the sample prepared via the traditional batch synthesis. Overall, we showed that a batch-guided screening enables rapid optimization of reaction parameters that can then be funneled into continuous synthesis. Our results show that a highly porous, crystalline HKUST-1 can be prepared within a few minutes with our millifluidic droplet technique, and we propose directions on further improvement in the productivity and quality of this MOF by optimization of the process parameters.

2. MATERIALS AND METHODS

2.1 Materials

All the chemicals and solvents except for DI water have been purchased commercially and used without any further purification. Benzene-1,3,5-tricarboxylic acid (95%, Millipore Sigma, USA), copper (II) nitrate hemi(pentahydrate) (*ACS reagent, ≥ 99.99% trace metal basis, Millipore Sigma, USA*), copper (II) acetate monohydrate (*99.99% trace metal basis, Millipore Sigma, USA*), sodium benzoate (≥ *99.0%, Millipore Sigma, USA*), benzoic acid (*ACS reagent, ≥ 99.5%, Millipore Sigma, USA*), N, N-dimethylformamide (≥ *99.7% for HPLC, VWR, USA*),ethanol (*200 Proof, 100%, VWR, USA*), dichloromethane (*ACS reagent, ≥ 99.5%, Millipore Sigma, USA*), silicone oil (*350 cSt at 25 °C, Millipore Sigma, USA*), liquid nitrogen (*Industrial grade, Airgas*).

2.2 Experimental workflow

The first phase of the experimental workflow involved conducting batch synthesis in small volumes to screen for the optimal reaction parameters for HKUST-1 synthesis. The second phase constituted

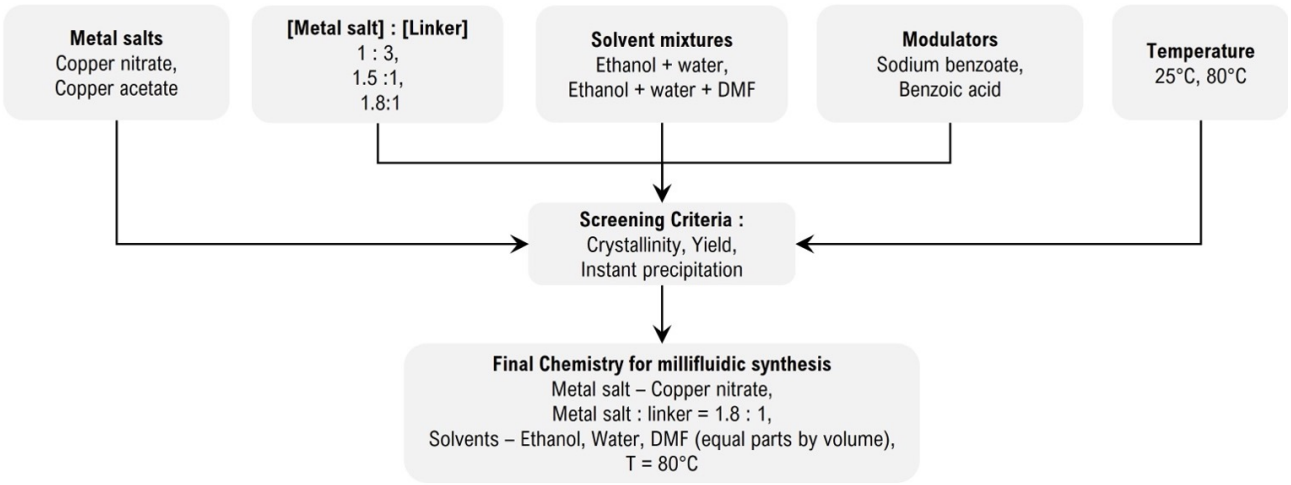

Figure 1: Optimization of reaction chemistry using Batch Synthesis. *Here DMF stands for N,N-dimethylformamide.*

incorporation of the optimized reaction chemistry in the continuous synthesis, wherein the quality and quantity of the resultant MOF was compared in detail with the corresponding batch synthesis. The batch process employs reaction under static conditions in an oven whereas the continuous synthesis technique involves the use of a millifluidic droplet reactor. The screening process developed for the chemistry optimization using batch synthesis is shown in Figure 1. The optimization process involved the generation of a multi-parameter space, wherein HKUST-1 was synthesized by varying the metal salts, metal salt to linker ratio, composition of solvent mixture, presence of modulators and reaction temperature. The details of the chemistry space are given in table 2 of §3.1. All the HKUST-1 samples synthesized using the parameter space were characterized using Powder X-Ray Diffraction and quantified for the yield. Some of the reactions generated HKUST-1 instantly after mixing the precursor solutions of metal salt and organic linker. This could be detrimental for the droplet generation stage of the millifluidic synthesis. The final chemistry, shown in Figure 1, was selected based on the crystallinity (comparison of experimental and simulated pattern), yield ($\geq$ 50%) and instant precipitation, if any.

Following the chemistry optimization, the synthesis of HKUST-1 using the millifluidic reactor and the corresponding batch process was performed. The experimental workflow for both processes are shown in Figure 2.

Aqueous solutions of benzene-1,3,5-tricarboxylic acid, commonly referred to as trimesic acid (H_3BTC, 0.319 g, 1.515 mmol) and copper (II) nitrate hemi(pentahydrate) ($Cu(NO_3)_2{\cdot}2.5H_2O$, 0.6 g, 2.58 mmol) were prepared in 15 ml of solvent mixture consisting of equal parts of deionized water (H_2O), ethanol (EtOH), and N, N-dimethylformamide (DMF) using a vortex mixer. Next, a precursor solution was prepared by mixing these solutions resulting in a metal salt to organic linker ratio of 1.8:1, which is shown to be the optimum ratio in this study and is also reported elsewhere [49]. Two such precursor solutions were prepared and one of them was subjected to the continuous synthesis route via the millifluidic reactor, the details of which are given in the next subsection. The other solution was sealed in a scintillation vial and kept in the oven (*VWR, Scientific Symphony 414004-616, Gravity Connection General Incubator*) at 80 °C for 10 hours. After the synthesis using both the routes, the product vial containing HKUST-1 suspended in the mother liquor solution was centrifuged three times (*Cole Parmer, Fixed Speed Centrifuge, Item #EW-17250-10, 3400 rpm*) with solvent decantation and an ethanol wash for each centrifugation step. Solid HKUST-1 thus obtained was dried in the oven at 95 °C for 12 hours to get the as-synthesized HKUST-1 powder. The activation of HKUST-1 was then performed to remove the solvent and organic linker molecules from the pores of the framework [50]. For activation, the dried MOF was immersed in a low boiling point solvent, dichloromethane [49], which replaced the high boiling point solvent, N, N-dimethylformamide. The duration of the solvent exchange step was 3 days, during which fresh solvent was replenished three times [49]. After this step, the solvent was decanted, and the MOF was heated to 100 °C in a vacuum oven (*Shel Lab 1407 Vacuum Oven- Analog Temperature Control*) for 12 hours to get the activated HKUST-1 samples.

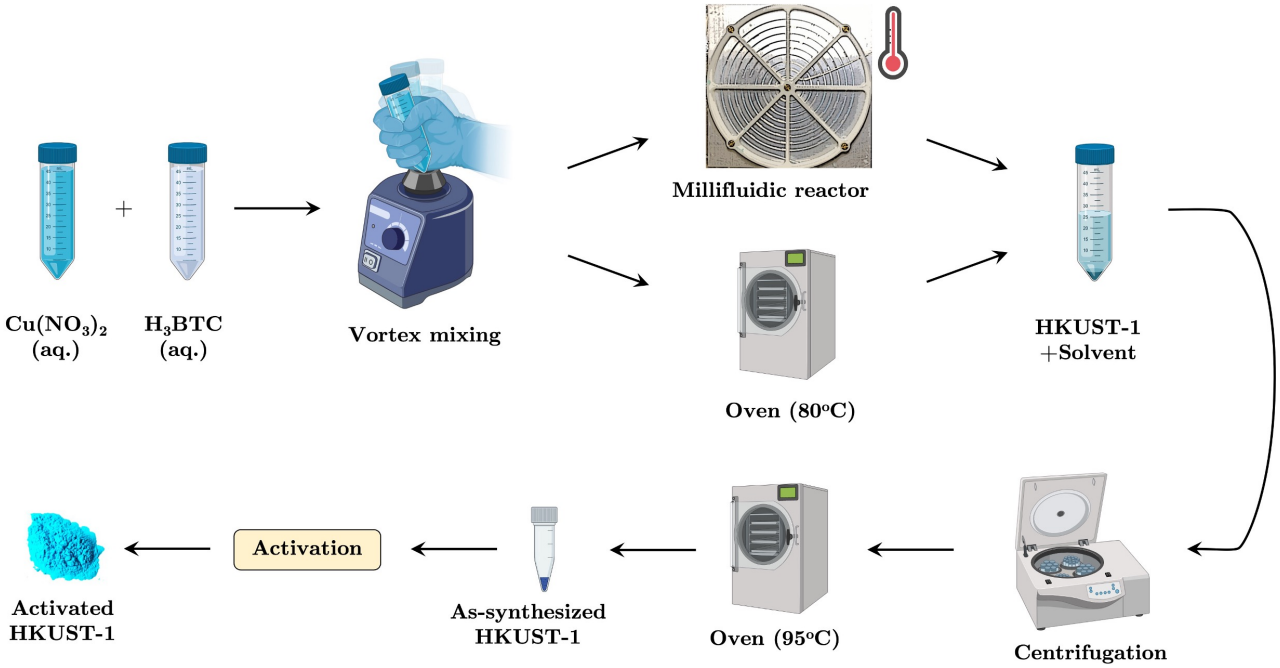

Figure 2: **Experimental workflow for Millifluidic and Batch synthesis**

2.3 Experimental setup and process parameters for continuous synthesis

The detailed schematic of the experimental setup of continuous synthesis using a Millifluidic reactor is shown in Figure 3(A). The top view of a section of the Millifluidic reactor is shown in Figure 3(B). In Figure 3(A) two syringes (*30 ml, BD Plastic*) filled with the reactant solution (30 ml) and silicone oil (15 ml) were installed on two syringe pumps (*Harvard PHD 2000*) for liquid infusion into PFA tubing (*1/32" ID × 1/16" OD, 2 m, Fluorotherm*) leading to a Tee junction (ETFE, 1/16" OD, IDEX). The flow of the precursor solution (50 μL/min) was kept parallel to the junction outlet, with the silicone oil being perpendicular to the junction outlet (25 μL/min) which gives a volumetric flow rate ratio of reactant solution to oil equal to 2:1. From initial trials, this ratio was found to result in a hydrodynamically stable flow, with homogeneous droplets and the absence of coalescence. This has also been observed by Bagi et al. [14], who used the same flow rate ratio of reactant solution to oil to generate droplets in a PTFE millifluidic tubing (*1/16" ID × 1/18" OD, 8 m*). Higher flow rate ratios of the two reagents resulted in non-uniform slugs with an irregular spacing after the T-junction. On the contrary, ratios corresponding to excess oil flow rates caused droplet coalescence in the tubing.

Thus, with an optimized solution to oil flow rate ratio of 2:1, a stable biphasic flow enters the millifluidic reactor in which PFA tubing is spirally fitted on a grooved aluminum block (*McMaster-Carr*) with the help of a 3D printed anchor. To get a residence time of 13 minutes for the volumetric flow rates mentioned above, the millifluidic reactor volume was set to ~990 μL. The residence time of 13 minutes was used to compare the results of our study with another study by Faustini et al. [39] which involved droplet-based continuous synthesis of HKUST-1.

The aluminum block was heated on a hot plate (*VWR*) with a set point temperature of 80 °C. Temperature values above this set point were also tried during the experiment runs; however, temperature values above 85 °C resulted in the generation of vapor bubbles in the reactor, leading to hydrodynamic failure. This could be due to the decomposition of N, N-dimethylformamide to formic acid and dimethylamine, wherein the formic acid can thermally decompose to produce gaseous carbon monoxide. Moreover, product collection was at atmospheric pressure and therefore, the operating pressure of 1 atm may have been lower than the bubble point pressure of the solvent mixture at 85 °C.

Entire heating setup was insulated using a custom-built box, with transparent window at the top for visualization. The 3D printed anchor ensures proper fitting of tubing within the grooves for uniform temperature distribution. Three thermocouples (*Omega, K-Type*) were installed at the entrance point,

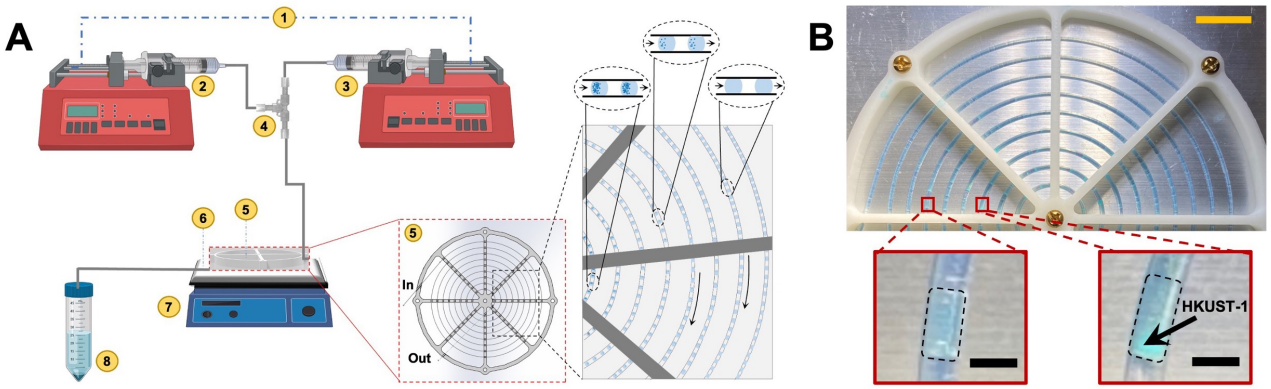

Figure 3: **Experimental setup for continuous synthesis of HKUST-1 using a millifluidic reactor. (A)** The setup includes: (1) syringe pump, (2) silicone oil in continuous phase, (3) reactant solution as dispersed phase, (4) ETFE Tee, (5) 3D printed anchor, (6) grooved aluminum block, (7) hot plate, and (8) product collection vial. **(B)** Image showing a section of Millifluidic reactor with insets showing droplets near the middle (LHS) and near the outlet (RHS) of reactor. Scale bar represents 1 cm (top panel) and 2 mm (insets). Blue colored particles indicating formation of HKUST-1 can be seen in the inset on RHS.

middle point, and exit point of the grooves to measure the temperature profiles (shown in figure S7, supplementary info) during the operation. The reactor product containing HKUST-1 particles in the mother liquor solution and silicone oil was collected in a centrifuge vial immersed in an ice bath to arrest the growth of HKUST-1 particles outside the millifluidic reactor. This product was then subjected to the various post-synthesis steps, as discussed in the previous section.

It can be seen from the insets of Figure 3B that the density of the particles and thereby the gradient of the blue color of the droplets intensify as the droplets traverse the spiral trajectory from the inlet to the reactor outlet. This confirmed the presence of reactive crystallization. Thus, visual monitoring was another beneficial feature of the setup.

2.4 Characterization

The activated samples were further characterized to assess the quality of the synthesized material. To characterize the crystallinity of HKUST-1 samples, Powder X-ray Diffraction (PXRD) data was collected using a Rigaku Miniflex II powder diffractometer. PXRD patterns were obtained for 2θ ranging from 3-50 ° with a step size of 0.02 °, and scan time of 5 min/deg. The X-ray source was Cu Kα radiation ($\lambda = 0.15418$ nm) with an anode voltage of 30 kV and a current of 15 mA. The PXRD data was collected using a position sensitive detector, the D/tex Ultra 250. The Fourier transform infrared spectroscopy (FTIR) spectrum was measured using a Thermo Scientific Nicolet iS 10 FTIR Spectrometer with a resolution of 0.4 cm^{-1} and for wavelengths ranging from 400 to 4000 cm^{-1}.

The nitrogen adsorption isotherms were measured monometrically using Autosorb iQ system (*Quantachrome Instruments, Boynton Beach, Florida, USA*) for the determination of the Brunauer-Emmett-Teller (BET) surface area of the HKUST-1 samples. The degassing of the sample was performed at a temperature of 200 °C for 6 hours. The analysis of the isotherm data was performed with ASiQWin software. To obtain the morphology of the MOF samples, Hitachi S/N 4300 scanning electron microscope (SEM) was used. The samples were fixed onto aluminum sample mounts using double sided carbon tape. The samples were then coated with a thin layer of Au/Pd. The SEM imaging was performed with aperture 4, at a voltage of 10 kV, an emission current of 83 μA, and a working distance of 17 mm. SEM images were acquired at three different magnifications of 300×, 1000× and 20,000×.

3. Results

3.1 Screening of reaction chemistry space using batch synthesis

HKUST-1 samples prepared using four different reaction reaction IDs (see Table 2) were screened to assess the crystallinity and instant precipitation. The second screening criteria refers to the blue precipitate formed immediately after mixing the metal salt and linker solutions, which was an important metric to decide whether clogging may occur in the millifluidic T-junction device when continuous synthesis was performed. This precipitate was quantified and characterized using PXRD, following the post-synthesis steps described in §2.2.

As can be seen in Table 2, all the IDs were subjected to three variations in the metal salt to linker ratios. Moreover, the deprotonation of the linker molecules was carried out by three different ways. The first method involved using two different solvent compositions in reaction ID 1. Nitrate anion, resulting from the dissociation of copper nitrate ($Cu(NO_3)_2{\cdot}2.5H_2O$) is a weak conjugate base of the strong nitric acid and is ineffective in the deprotonation of trimesic acid. Thus, the addition of the solvent N, N-dimethylformamide (DMF) to the solvent mixture of ethanol (EtOH) and water (H_2O) can mitigate this problem. The thermal decomposition of DMF results in the release of the organic base dimethylamine, which leads to the faster deprotonation of trimesic acid [1]. Thus, in the reaction ID 1, two solvent compositions, with and without DMF, were used to compare the crystallinity and yield of the MOF synthesized at 25 °C and 80 °C.

Table 2: **Reaction chemistry parameters space.** (**MS** is metal Salt, **L** is linker, **T** is temperature, $\mathbf{t}_r$ is residence time in hours, Inst. is instantaneous, **Mod** is modulator, **x** is mole fraction, BA is benzoic acid, B- is sodium benzoate, and **n** is number of samples.)

ID	MS	[L]	MS:L	T (t_r)	Solvent	Mod	L:Mod	x_{BA}	n
1.	$Cu(NO_3)_2$ $\cdot 2.5H_2O$	0.09 M	1:3, 1.5:1, 1.8:1	25 °C (Inst.), 25°C (10), 80°C (10)	EtOH:H_2O:DMF EtOH:H_2O	–	–	–	18
2.	$Cu(CO_2CH_3)_2$ $\cdot H_2O$	0.09 M	1:3, 1.5:1, 1.8:1	25°C (Inst.)	EtOH:H2O	–	–	–	3
3.	$Cu(NO_3)_2$ $\cdot 2.5H_2O$	0.03 M	1:3, 1.5:1, 1.8:1	25°C (Inst.)	EtOH:H2O	B-	1:1, 1:3	–	6
4.	$Cu(NO_3)_2$ $\cdot 2.5H_2O$	0.03 M	1:3, 1.5:1, 1.8:1	25°C (Inst.)	EtOH:H2O	BA + B-	1:1, 1:3	0.33, 0.5, 0.66	18

The second method to induce deprotonation of the linker involved the use of copper acetate ($Cu(CO_2CH_3)_2{\cdot}H_2O$) as the metal salt because acetate anion is a strong conjugate base of the weak acetic acid (reaction ID 2). Thus, in this case, the solvent mixture consisted of ethanol and water as the use of DMF was not necessary. It was observed that upon mixing the solutions of copper acetate and trimesic acid for all the three MS: L ratios, aqua blue colored precipitate was formed instantly, which was confirmed to be HKUST-1 from PXRD patterns as shown in Figure S1 (Supplementary Information). Since, instantaneous formation of HKUST-1 was confirmed with copper acetate as the metal salt, the reaction ID 2 was not used for the millifluidic synthesis because it would lead to the clogging of the T-junction during the course of the experiments.

The reaction IDs 3 and 4 involved the use of the modulators such as basic sodium benzoate and buffer solutions of benzoic acid and sodium benzoate respectively, to induce linker deprotonation [51]. Moreover, the linker to modulator ratio was varied to be 1:1 and 1:3 in both the IDs and the pH of the buffer solution was adjusted by modifying the mole fraction of benzoic acid (0.33, 0.5 and 0.66) [51] in reaction ID 4. Similar to the results of reaction ID 2, both the IDs caused instantaneous

Table 3: **Optimization of reaction reaction ID 1.** MS is metal salt, L is linker, T is temperature, tr is residence time in hours, Inst. is instantaneous, x is no product, o is sticky blue precipitate (yield could not be quantified), ✓ is HKUST-1 (✓: *optimized condition*), # is blue and white particles (low yield for PXRD), ✓* is blue particles (low yield for PXRD).

Solvent		**EtOH:H_2O:DMF (1:1:1)**			**EtOH:H_2O (1:1)**		
T		25 °C	25 °C	80 °C	25 °C	25 °C	80 °C
(t_r)		(Inst.)	(10 hrs)	(10 hrs)	(Inst.)	(10 hrs)	(10 hrs)
MS:L	**1:03**	x	x	✓	x	x	x
	1.5:1	x	o	✓	x	#	✓*
	1.8:1	x	o	✓	x	#	✓*

formation of HKUST-1 for all variations in MS: L, L:Mod and benzoic acid equivalents as can be seen in Figures S2 and S3 (Supplementary Information).Therefore, both reaction IDs 3 and 4 were discarded as conditions for the millifluidic synthesis.

It should be noted that the reaction ID 1 did not cause formation of HKUST-1 upon instant mixing of the reactant solutions for the two solvent compositions and the three MS: L ratios, suggesting it might be a suitable candidate for continuous synthesis. Therefore, the reaction ID 1 was subjected to further screening to obtain the optimal reaction chemistry as discussed in §3.2.

3.2 Batch optimization of reaction ID-1

In table 3, we show the conditions tested for reaction ID 1, and the key observations. The characterization using PXRD of the HKUST-1 samples obtained using reaction ID 1 was performed for the solvent composition of ethanol, water and DMF at the temperature of 80 °C and reaction time of 10 hours as all the other conditions either resulted in no product or unquantifiable low yield of the product, as can be seen in table 3. Moreover, it should be noted that for the solvent composition of ethanol and water, at the condition of 80 °C (10 hours), the MS: L ratios of 1.5:1 and 1.8:1 resulted in blue particles, but the yield was insufficient for PXRD characterization.

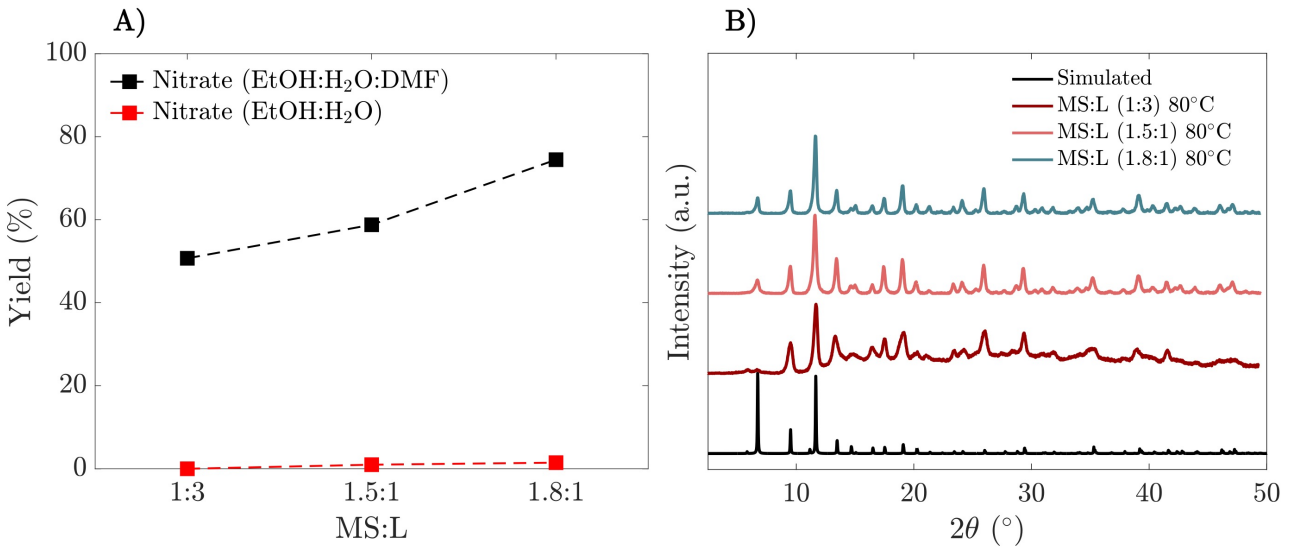

Figure 4: **Physical characterization of HKUST-1 samples synthesized via batch processes. (A)** Yield of HKUST-1 using solvent mixtures with and without DMF and **(B)** PXRD of HKUST-1 synthesized at 80 °C (10 hours) and solvent mixture of EtOH:H_2O:DMF.

The yield of the blue particles synthesized using both solvent compositions at the temperature of 80 °C and reaction time of 10 hours was quantified and is shown in Figure 4(A). The yield for the

solvent mixture of ethanol and water was less than 2% for all three MS: L ratios. In stark contrast, the yield for the solvent mixture of ethanol, water and DMF increased from 50% at the MS: L ratio of 1:3 to 75% at the MS: L ratio of 1.8:1. Thus, the three samples obtained using this solvent mixture were also subjected to PXRD characterization, as is shown in Figure 4(B). The MS: L ratio of 1.5:1 and 1.8:1 resulted in highly crystalline HKUST-1, as opposed to the poor crystallinity of the sample synthesized using MS:L of 1:3.

Therefore, the optimized reaction chemistry selected from the batch-screening process involved using copper nitrate as the metal salt, with metal salt to linker ratio of 1.8:1 and solvent mixture containing equal parts by volume of ethanol, water and DMF. This reaction chemistry is highlighted in red in table 3. The batch guided screening also indicates that the reaction chemistry of a batch process may not be necessarily transferable to continuous flow synthesis processes, particularly those involving microfluidic and millifluidic reactors.

3.3 Continuous millifluidic synthesis of HKUST-1

In this section, we discuss the characterization results of HKUST-1 synthesis using the droplet millifluidic reactor at the optimal condition identified in the batch screening. Specifically, we discuss the crystallinity, chemical bond identification, particle morphology, size distribution, and yield of HKUST-1 samples synthesized using both the batch and continuous techniques. We elucidate the differences observed in the properties using crystallization mechanism of HKUST-1 which was reported elsewhere [52, 53].

Crystallinity. We performed PXRD to confirm the crystallinity of the synthesized HKUST-1 samples. The PXRD patterns for samples obtained from the batch and continuous processes are shown in figure 5(A). We confirmed that the phases of the samples synthesized via both techniques were indeed crystalline HKUST-1 by comparing their PXRD patterns with the simulated pattern of the same, which was acquired from the Powder Diffraction database (PDF 00-065-1028) (PDF4+, Release 2015, International Centre of Diffraction Data, ICDD, Pennsylvania, USA).

Chemical bonds identification. FTIR spectra were used to identify the chemical bonds between different atoms of the structure of the HKUST-1 samples (see Figure 5(B)). The peaks with labels 'a' and 'b' at the wavenumbers of 1646 cm^{-1} and 1550 cm^{-1} respectively, correspond to asymmetric COO^- vibrations [54–56].

Similarly, the symmetric COO^- vibrations are captured by the peaks labeled 'c' and 'd', corresponding to the wavenumbers of 1370 cm^{-1} and 1445 cm^{-1} respectively [54–56]. The vibration of the Cu-O bond is labeled as peak 'e' at the wavenumber of 730 cm^{-1} [56]. Therefore, the presence of the labeled peaks in the spectra substantiated the coordination of the carboxylate binding groups to the copper ions to form the secondary building units of HKUST-1. The peaks representing vibrations of the benzene ring are also present in spectra. Furthermore, there are no peaks corresponding to H_3BTC [57] or DMF [58] that could be trapped in the pores of the framework, confirming the successful activation of the samples. The detailed classification of the IR peaks is given in table S1 (supplementary information).

Morphology and particle size distribution. After confirming the crystallinity and chemical bonds of the samples, SEM was performed to determine the morphology and particle size of the HKUST-1 crystals. The average particle size of HKUST-1 crystals synthesized using batch process is 14.8±8.5 μm. The morphology of most of the particles is octahedral, which can be seen in figure 5(C). These observations are in line with the particle size and morphology of bulk HKUST-1 crystals synthesized using solvothermal batch process in the literature. [59].

The average particle size of the crystals synthesized within the droplets of the millifluidic reactor is 14.5±11.6 μm, which is in excellent agreement with the samples obtained from the batch process. The bulk particles of the samples synthesized by the continuous process have a polyhedral morphology, with sharp edges as can be observed from Figure 5(D). Furthermore, most of the particles tend to attain an octahedral morphology indicating incomplete growth for a low residence time of 13 minutes. It is noteworthy that particulate clusters with irregular morphology were also observed in the vicinity of the bulk particles. We hypothesize that these clusters formed within a short residence time are the growing nuclei of this MOF. The rationale behind this hypothesis is based on a study of the

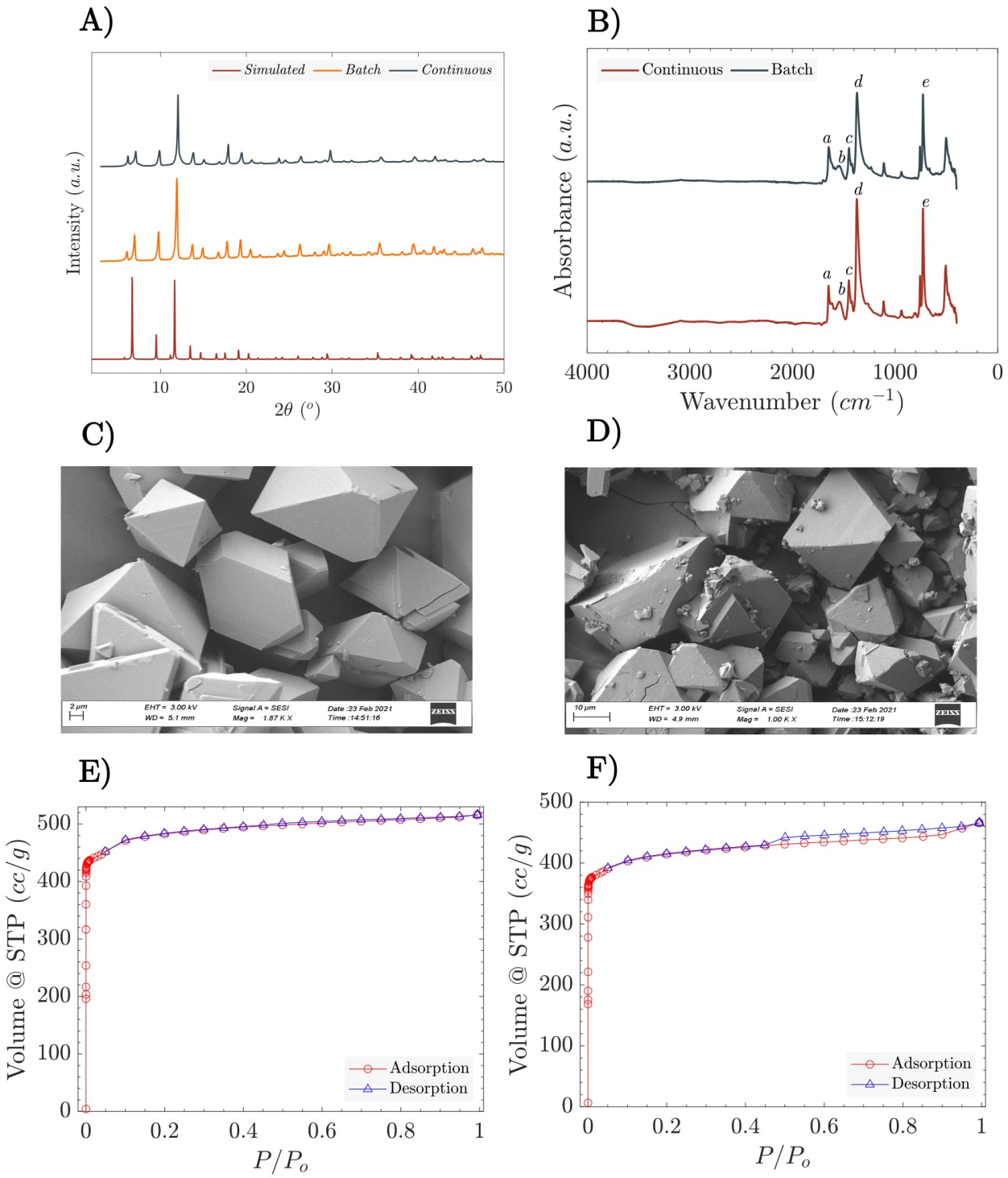

Figure 5: **Physical characterization of HKUST-1 samples synthesized via batch and continuous processes.** **(A)** Powder X-ray diffraction (PXRD) patterns of samples compared with standard simulated pattern [60] of HKUST-1. **(B)** Fourier transform infrared spectra (FTIR) for samples; refer to the main text for a description of the peaks labeled a-f in the plots. Scanning Electron Microscopy (SEM) images of HKUST-1 synthesized by **(C)** batch process and **(D)** continuous process. Nitrogen adsorption-desorption isotherms at 77 K for HKUST-1 samples synthesized from **(E)** batch process and **(F)** continuous process.

crystallization kinetics of HKUST-1 for a temperature range of 85-125°C by Millange et al. [52]. They showed that the nucleation is the rate-controlling step in the crystallization at different temperatures and occurs instantaneously without an induction period, extending into the growth regime. Thus, the experimental evidence from SEM images and observations of Millange et al. [52] corroborate the argument of incomplete growth at the nucleation sites for a short residence time of 13 minutes. No such particulate clusters can be seen in Figure 5(C) for the samples synthesized using batch process. This indicates that the slow crystallization process under solvothermal batch conditions with long residence time results in the complete growth of MOF particles.

Porosity and surface area. We investigated the porosity and BET surface area of HKUST-1 samples obtained using both processes. These values were obtained from the nitrogen adsorption-desorption isotherms for the batch process sample (see Figure 5(E)) and continuous process sample (see Figure 5(F)). The isotherm of Figure 5(E) is a Type-I isotherm, indicating the presence of micropores. The average BET surface area and micropore volume determined from this isotherm were 1761±137 m^2/g and 0.56±0.03 cm^3/g, respectively. These observations agree with the nitrogen sorption measurements reported in the literature [18, 21, 32, 48].

The isotherm shown in Figure 5(F) for the flow synthesized sample is also a Type-I isotherm, confirming micropores in the structure. Interestingly, there is a small hysteresis loop between the adsorption and desorption experiments for the P/P_o values in the range of 0.5-0.9. This hysteresis loop is of Type H4 [61] and is a characteristic of some degree of mesoporosity in the structure [61]. The aggregation of small particles often leads to inter-grain voids, which cause the formation of mesopores [62]. The presence of such voids may be rationalized from the SEM image of Figure 5(D), which shows aggregated particulate clusters on the surface of bulk crystals. Such type of isotherm behavior has been observed previously in the literature for HKUST-1 crystals and composite materials [35, 62, 63]. The average BET surface area and micropore volume for the flow-synthesized sample were 1615±106 m^2/g and 0.55±0.04 cm^3/g, respectively. The reduced surface area for the samples synthesized by the continuous process is supported by the incomplete growth of HKUST-1 particles within a short residence time of 13 minutes.

Yield. We have also quantified the amount of HKUST-1 synthesized using the droplet millifluidic reactor with a residence time of 13 minutes. The amount of the as-synthesized HKUST-1 crystals was 62±9.5mg, which reduced to 49.7±6.4 mg after activation. We showed that the change in the amount of the sample before and after activation was insignificant ($p > 0.05$) using ANOVA test . The yield based on the complete conversion of the limiting reactant (H_3BTC) was 15%. On the contrary, we did not observe the formation of HKUST-1 crystals by the batch process within a short residence time of 13 minutes.

4. Discussion

Batch-synthesis screening is a promising approach for selecting conditions for continuous millifluidic synthesis. A major challenge in conducting droplet-based millifluidic synthesis of MOFs involves not only optimization of reaction parameters but also optimization of multiple flow conditions to yield stable droplet trains of desirable reactor volume, spacing and residence time. Given this vast parametric space, it is useful to seek alternate approaches that can rapidly select conditions suitable for millifluidic droplet reactors. In this regard, our study shows that batch-synthesis screening enables rapid selection of conditions based on crystallinity, yield and precipitation time. We screened a total of 45 conditions and found one reaction chemistry that has prolonged induction time for precipitation, enabling continuous droplet production without formation of a precipitate at the T-junction nozzle.

In this section, we have highlighted the main features of reactive crystallization under flow conditions and rationalized the observations of physical properties of HKUST-1 samples prepared in the droplet millifluidic reactor. We also performed a detailed comparative analysis of the results of this work and that of Faustini et al. [39].

4.1 Formation of bulk HKUST-1 crystals within minutes

The nucleation rate at a given temperature is a function of supersaturation of the solution [64]. Since the same concentration of the reagents is used for both synthesis processes, the supersaturation at the beginning of the reactive crystallization is equal for both techniques. However, the fluid inside a millifluidic droplet is rapidly mixed due to chaotic advection [65,66] which has two-fold consequences: (i) the heat transfer rate is enhanced, leading to faster formation of HKUST-1 nuclei [14] and (ii) higher mass transfer rate accelerating the transport of growth units to the nucleation sites. Thus, HKUST-1 crystals were observed even for the short residence times of 13 minutes with a 15% yield, as opposed to none for the batch process with the same residence time. This phenomenon is depicted in Figure 6(A).

Interestingly, an increase in the rate of growth depletes the supersaturation of the solution [45]. As a result, the rate of primary nucleation decreases, leading to higher average particle size [45]. This phenomenon explains the particle size of bulk HKUST-1 crystals obtained by the continuous process to be equivalent to the average size of particles obtained by the batch process, wherein the high residence time results in the formation of big crystals. The average particle size observed in this work is nearly the same as that obtained by Faustini et al. [39], using the microfluidic droplet approach.

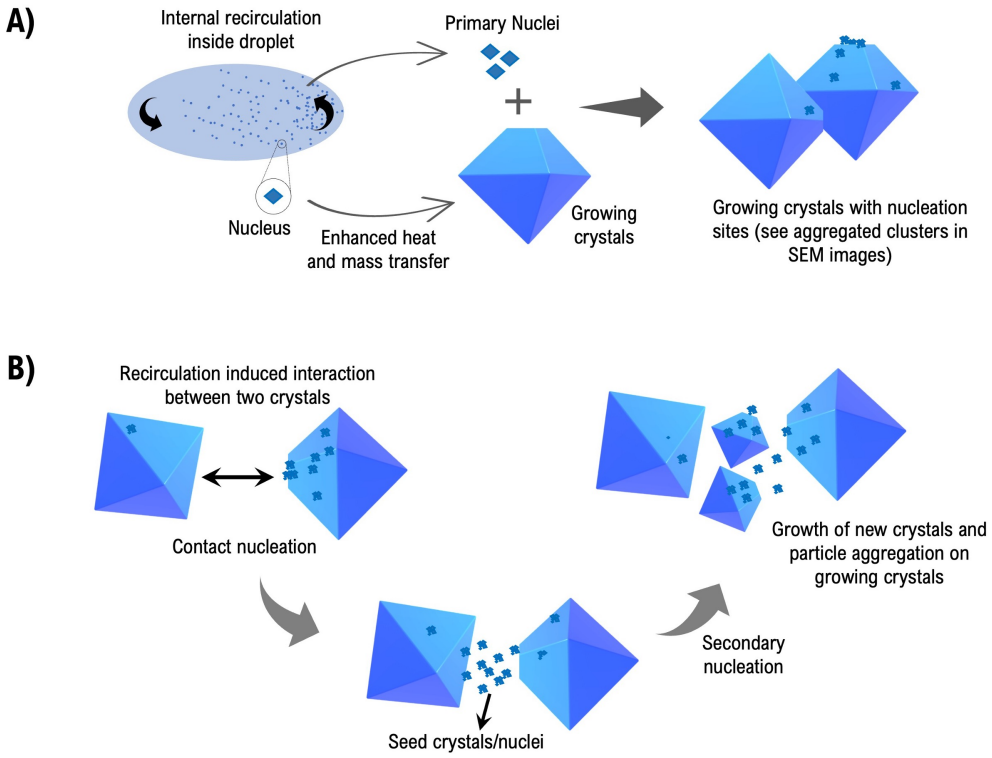

Figure 6: **Crystallization mechanisms inside a millifluidic droplet. (A)** Enhanced nucleation and crystal growth inside a millifluidic droplet. **(B)** Secondary nucleation and crystal growth induced by interaction of recirculating crystals.

Moreover, the presence of HKUST-1 crystals circulating with the flow inside the droplets may lead to contact nucleation, a type of secondary nucleation that results from the interaction of two crystals [64]. As secondary nucleation occurs at lower levels of supersaturation [64], it generates secondary nuclei within the droplets. Short residence time renders the incomplete growth of the secondary nuclei. This phenomenon is depicted in Figure 6(B). Thus, in addition to the previously mentioned observations of Millange et al. [52] in §3.3, the possibility of secondary nucleation could also justify the presence of aggregates on the surface of the bulk crystals seen in figure 5(D). Furthermore, such aggregation reduced the BET surface area of the samples obtained in the millifluidic droplet reactor. The surface area values of 1615±106 m^2/g for the flow-synthesized samples (13 minutes) and 1761±137 m^2/g for the batch samples (10 hours) reported in this work are significantly higher than

the corresponding values reported by Faustini et al. [39], who obtained the value of ∼600 m^2/g for the flow samples (12 minutes) and 1664 m^2/g for the batch samples (24 hours). However, they reported a much higher BET surface area of 1911 m^2/g for the sample synthesized using continuous process with a residence time of 3 minutes. However, they did not provide any explanation for the three-fold decrease in the BET surface area upon increasing the residence time from 3 minutes to 12 minutes.

4.2 Comments on the yield of HKUST-1

In this work, we obtained a yield of ∼15% based on the limiting reactant and ∼12% based on the complete conversion of copper for the HKUST-1 crystals synthesized using droplet millifluidic reactor. In sharp contrast, Faustini et al. [39] showed a yield of ∼68% (based on the copper conversion) for HKUST-1 synthesis via microfluidic droplet approach for a residence time of 12 minutes and a reaction temperature of 90 °C. The total flow rate corresponding to the reported residence time of 12 minutes was 6 μL/min. Thus, with the reactor volume of 243.22 μL (PFA tubing ID=0.508 mm, length = 1.2 m), the high yield reported by Faustini et al. [39] can be attributed to the actual residence time of ∼40 minutes (nearly thrice of the residence time used in the current study). Moreover, the synthesis temperature used by Faustini et al. [39] was 90 °C which exceeds the reaction temperature in the present work by 10 °C. The rate constants for nucleation (k_N) and crystal growth (k_G) for temperature of 90 °C were 0.014 min^{-1} and 0.044 min^{-1} respectively based on the crystallization kinetics of HKUST-1 performed by Millange et al. [53]. For the present work, these values are twice of the values of k_N (=0.007 min^{-1}) and k_G (=0.024 min^{-1}) for the reaction temperature of 80 °C (see details in §S5 of supplementary info). A decrease of 10 °C in the reaction temperature reduces the rate of crystallization process by 50%. Thus, lower yield of our work can be justified when compared to the work of Faustini et al. [39].

4.3 On improving the process productivity

Based on a detailed comparison of the samples synthesized in this study using flow and batch techniques as well as comparison with the previous literature study [39], we suggest that the process parameters which should be optimized to improve the yield and productivity of HKUST-1 are the residence time, temperature, and inner diameter of tubing. These values should be carefully chosen to maximize the space-time yield of HKUST-1, without compromising the surface area and microporosity of the material. The experimental techniques such as time-resolved X-ray diffraction can be used to understand the reaction kinetics within a droplet reactor [14, 45]. The calculations of the bubble point pressure of the solvent mixture should also be performed to yield an accurate backpressure which should be used for the operation to ensure liquid phase in the reactor. This will allow the use of higher temperatures to increase the reaction rate, while maintaining a stable liquid phase for the droplets. Moreover, computational fluid dynamics can be used to optimize the tube dimensions, reactor volume and flow rates. After the optimization of the reaction and process parameters for a single droplet millifluidic reactor, a detailed investigation for the parallelization of such reactors should be performed experimentally with fine tuning of the process control parameters. We propose that the current droplet millifluidic reactor can be easily integrated in such parallelization schemes due to the novel configuration, which is free of the oil bath, commonly used in other studies of MOF crystallization [39, 40]. This makes the entire setup easy-to-assemble and easy-to-clean, thus making the reactor reusable.

5. Conclusions

In conclusion, we demonstrate a novel configuration of a droplet millifluidic reactor for the continuous synthesis of high-quality crystals of HKUST-1, comparable to the sample prepared via the traditional batch process. We also generated a multidimensional reaction space which was screened using batch synthesis for the selection of the optimum chemistry. This novel screening study concluded that the rate of linker deprotonation and supersaturation of the solution can be significantly increased by using different metal salts and modulators in batch reactors, leading to instant precipitation. However,

the main outcome of this investigation is that such reaction parameters are not entirely transferable to be used in the millifluidic reactors, which can be prone to clogging in the droplet generation stage. The highlight of our study is an easy-to-assemble, reusable and oil-bath free reactor that can synthesize HKUST-1 within a few minutes of residence time. We have also evaluated the textural properties and morphology of the samples and have performed an in-depth comparison of the same with the corresponding properties of the samples synthesized using the batch process. Through such a comparison, we have highlighted the key process parameters that need to be optimized for the scaled-up synthesis of HKUST-1. A detailed investigation of the crystallization kinetics, tuning of residence time and reactor volume for the millifluidic droplet reactor should be carried out in future to optimize the productivity of a single reactor. Therefore, this study has tremendous potential in scaling-up the synthesis of HKUST-1. The synthesis of other MOFs should also be explored in such reactors to make the process more versatile.

6. Author Contributions

RS designed and performed all the batch and continuous flow experiments, performed the physical characterization of MOF samples, analyzed the data and wrote the original draft of the manuscript. **TE** assisted in batch experiments, FTIR characterization of MOF samples and in the analysis of data. **DU** supervised PXRD characterization and data analysis for the same. **HH** performed BET surface area measurements. **AC** guided the design of batch experiments. **CCC** acquired the funding, reviewed and edited the manuscript. **SV** conceptualized the project, designed the experiments, analyzed the data, reviewed and edited the manuscript.

7. Acknowledgements

The authors thank the financial support of the Jack Maddox Foundation. We are grateful to Dr. Bo Zhao for performing the Scanning Electron Microscopy on HKUST-1 samples and for useful discussions regarding the analysis of SEM images.

References

[1] Omar M Yaghi, Markus J Kalmutzki, and Christian S Diercks. *Introduction to reticular chemistry: metal-organic frameworks and covalent organic frameworks*. John Wiley & Sons, 2019.

[2] Hiroyasu Furukawa, Kyle E Cordova, Michael O'Keeffe, and Omar M Yaghi. The chemistry and applications of metal-organic frameworks. *Science*, 341(6149):1230444, 2013.

[3] Markus J Kalmutzki, Nikita Hanikel, and Omar M Yaghi. Secondary building units as the turning point in the development of the reticular chemistry of mofs. *Science advances*, 4(10):eaat9180, 2018.

[4] Ashlee J Howarth, Yangyang Liu, Peng Li, Zhanyong Li, Timothy C Wang, Joseph T Hupp, and Omar K Farha. Chemical, thermal and mechanical stabilities of metal–organic frameworks. *Nature Reviews Materials*, 1(3):1–15, 2016.

[5] JeongYong Lee, Omar K Farha, John Roberts, Karl A Scheidt, SonBinh T Nguyen, and Joseph T Hupp. Metal–organic framework materials as catalysts. *Chemical Society Reviews*, 38(5):1450–1459, 2009.

[6] Lauren E Kreno, Kirsty Leong, Omar K Farha, Mark Allendorf, Richard P Van Duyne, and Joseph T Hupp. Metal–organic framework materials as chemical sensors. *Chemical reviews*, 112(2):1105–1125, 2012.

[7] Meili Ding, Robinson W Flaig, Hai-Long Jiang, and Omar M Yaghi. Carbon capture and conversion using metal–organic frameworks and mof-based materials. *Chemical Society Reviews*, 48(10):2783–2828, 2019.

[8] Markus J Kalmutzki, Christian S Diercks, and Omar M Yaghi. Metal–organic frameworks for water harvesting from air. *Advanced Materials*, 30(37):1704304, 2018.

[9] Nikita Hanikel, Mathieu S Prévot, Farhad Fathieh, Eugene A Kapustin, Hao Lyu, Haoze Wang, Nicolas J Diercks, T Grant Glover, and Omar M Yaghi. Rapid cycling and exceptional yield in a metal-organic framework water harvester. *ACS central science*, 5(10):1699–1706, 2019.

[10] Wentao Xu and Omar M Yaghi. Metal–organic frameworks for water harvesting from air, anywhere, anytime. *ACS central science*, 6(8):1348–1354, 2020.

[11] Paulina A Kobielska, Ashlee J Howarth, Omar K Farha, and Sanjit Nayak. Metal–organic frameworks for heavy metal removal from water. *Coordination Chemistry Reviews*, 358:92–107, 2018.

[12] Timur Islamoglu, Zhijie Chen, Megan C Wasson, Cassandra T Buru, Kent O Kirlikovali, Unjila Afrin, Mohammad Rasel Mian, and Omar K Farha. Metal–organic frameworks against toxic chemicals. *Chemical Reviews*, 120(16):8130–8160, 2020.

[13] Jianwei Ren, Xoliswa Dyosiba, Nicholas M Musyoka, Henrietta W Langmi, Mkhulu Mathe, and Shijun Liao. Review on the current practices and efforts towards pilot-scale production of metal-organic frameworks (mofs). *Coordination Chemistry Reviews*, 352:187–219, 2017.

[14] Sujay Bagi, Ashley M Wright, Julius Oppenheim, Mircea Dincă, and Yuriy Román-Leshkov. Accelerated synthesis of a ni2cl2 (btdd) metal–organic framework in a continuous flow reactor for atmospheric water capture. *ACS Sustainable Chemistry & Engineering*, 9(11):3996–4003, 2021.

[15] Yu-Ri Lee, Jun Kim, and Wha-Seung Ahn. Synthesis of metal-organic frameworks: A mini review. *Korean Journal of Chemical Engineering*, 30(9):1667–1680, 2013.

[16] Sung-Hwa Jhung, Jin-Ho Lee, and Jong-San Chang. Microwave synthesis of a nanoporous hybrid material, chromium trimesate. *Bulletin of the Korean Chemical Society*, 26(6):880–881, 2005.

[17] Jung-Sik Choi, Won-Jin Son, Jahoen Kim, and Wha-Seung Ahn. Metal–organic framework mof-5 prepared by microwave heating: Factors to be considered. *Microporous and Mesoporous Materials*, 116(1-3):727–731, 2008.

[18] Nazmul Abedin Khan, Enamul Haque, and Sung Hwa Jhung. Rapid syntheses of a metal–organic framework material cu 3 (btc) 2 (h 2 o) 3 under microwave: a quantitative analysis of accelerated syntheses. *Physical Chemistry Chemical Physics*, 12(11):2625–2631, 2010.

[19] Nazmul Abedin Khan and Sung Hwa Jhung. Phase-transition and phase-selective synthesis of porous chromium-benzenedicarboxylates. *Crystal growth & design*, 10(4):1860–1865, 2010.

[20] Nazmul Abedin Khan and Sung Hwa Jhung. Synthesis of metal-organic frameworks (mofs) with microwave or ultrasound: Rapid reaction, phase-selectivity, and size reduction. *Coordination Chemistry Reviews*, 285:11–23, 2015.

[21] Nazmul Abedin Khan and Sung-Hwa Jhung. Facile syntheses of metal-organic framework cu 3 (btc) 2 (h 2 o) 3 under ultrasound. *Bulletin of the Korean Chemical Society*, 30(12):2921–2926, 2009.

[22] Ulrich Mueller, Hermann Puetter, Michael Hesse, Markus Schubert, Helge Wessel, Juergen Huff, and Marcus Guzmann. Method for electrochemical production of a crystalline porous metal organic skeleton material, June 28 2011. US Patent 7,968,739.

[23] Alberto Martinez Joaristi, Jana Juan-Alcañiz, Pablo Serra-Crespo, Freek Kapteijn, and Jorge Gascon. Electrochemical synthesis of some archetypical zn2+, cu2+, and al3+ metal organic frameworks. *Crystal Growth & Design*, 12(7):3489–3498, 2012.

[24] Hongwei Yang, Samuel Orefuwa, and Andrew Goudy. Study of mechanochemical synthesis in the formation of the metal–organic framework cu3 (btc) 2 for hydrogen storage. *Microporous and mesoporous materials*, 143(1):37–45, 2011.

[25] Toma N Glasnov and C Oliver Kappe. Microwave-assisted synthesis under continuous-flow conditions. *Macromolecular rapid communications*, 28(4):395–410, 2007.

[26] Markus Damm, Toma N Glasnov, and C Oliver Kappe. Translating high-temperature microwave chemistry to scalable continuous flow processes. *Organic Process Research & Development*, 14(1):215–224, 2010.

[27] Roman Morschhäuser, Matthias Krull, Christoph Kayser, Cornelia Boberski, Ralf Bierbaum, Peter A Püschner, Toma N Glasnov, and C Oliver Kappe. Microwave-assisted continuous flow synthesis on industrial scale. *Green Processing and Synthesis*, 1(3):281–290, 2012.

[28] Michael P Batten, Marta Rubio-Martinez, Trevor Hadley, Keri-Constanti Carey, Kok-Seng Lim, Anastasios Polyzos, and Matthew R Hill. Continuous flow production of metal-organic frameworks. *Current Opinion in Chemical Engineering*, 8:55–59, 2015.

[29] Peter W Dunne, Edward Lester, and Richard I Walton. Towards scalable and controlled synthesis of metal–organic framework materials using continuous flow reactors. *Reaction Chemistry & Engineering*, 1(4):352–360, 2016.

[30] Amanda A. Volk, Zachary S. Campbell, Malek Y.S. Ibrahim, Jeffrey A. Bennett, and Milad Abolhasani. Flow chemistry: A sustainable voyage through the chemical universe en route to smart manufacturing. *Annual Review of Chemical and Biomolecular Engineering*, 13(1), 2022.

[31] Ryan L. Hartman, Jonathan P. McMullen, and Klavs F. Jensen. Deciding whether to go with the flow: Evaluating the merits of flow reactors for synthesis. *Angewandte Chemie International Edition*, 50(33):7502–7519, 2011.

[32] Miquel Gimeno-Fabra, Alexis S Munn, Lee A Stevens, Trevor C Drage, David M Grant, Reza J Kashtiban, Jeremy Sloan, Edward Lester, and Richard I Walton. Instant mofs: continuous synthesis of metal–organic frameworks by rapid solvent mixing. *Chemical Communications*, 48(86):10642–10644, 2012.

[33] Paul M Schoenecker, Grace A Belancik, Bogna E Grabicka, and Krista S Walton. Kinetics study and crystallization process design for scale-up of uio-66-nh2 synthesis. *AIChE Journal*, 59(4):1255–1262, 2013.

[34] Colin McKinstry, Russell J Cathcart, Edmund J Cussen, Ashleigh J Fletcher, Siddharth V Patwardhan, and Jan Sefcik. Scalable continuous solvothermal synthesis of metal organic framework (mof-5) crystals. *Chemical Engineering Journal*, 285:718–725, 2016.

[35] Ki-Joong Kim, Yong Jun Li, Peter B Kreider, Chih-Hung Chang, Nick Wannenmacher, Praveen K Thallapally, and Ho-Geun Ahn. High-rate synthesis of cu–btc metal–organic frameworks. *Chemical Communications*, 49(98):11518–11520, 2013.

[36] Peter A Bayliss, Ilich A Ibarra, Eduardo Pérez, Sihai Yang, Chiu C Tang, Martyn Poliakoff, and Martin Schröder. Synthesis of metal–organic frameworks by continuous flow. *Green Chemistry*, 16(8):3796–3802, 2014.

[37] Marta Rubio-Martinez, Michael P Batten, Anastasios Polyzos, Keri-Constanti Carey, James I Mardel, Kok-Seng Lim, and Matthew R Hill. Versatile, high quality and scalable continuous flow production of metal-organic frameworks. *Scientific Reports*, 4(1):1–5, 2014.

[38] Steve Waitschat, Michael T Wharmby, and Norbert Stock. Flow-synthesis of carboxylate and phosphonate based metal–organic frameworks under non-solvothermal reaction conditions. *Dalton Transactions*, 44(24):11235–11240, 2015.

[39] Marco Faustini, Jun Kim, Guan-Young Jeong, Jin Yeong Kim, Hoi Ri Moon, Wha-Seung Ahn, and Dong-Pyo Kim. Microfluidic approach toward continuous and ultrafast synthesis of metal–organic framework crystals and hetero structures in confined microdroplets. *Journal of the American Chemical Society*, 135(39):14619–14626, 2013.

[40] Lorena Paseta, Beatriz Seoane, Daniel Julve, Victor Sebastian, Carlos Téllez, and Joaquín Coronas. Accelerating the controlled synthesis of metal–organic frameworks by a microfluidic approach: a nanoliter continuous reactor. *ACS applied materials & interfaces*, 5(19):9405–9410, 2013.

[41] Sachin R Jambovane, Satish K Nune, Ryan T Kelly, B Peter McGrail, Zheming Wang, Manjula I Nandasiri, Shanta Katipamula, Cameron Trader, and Herbert T Schaef. Continuous, one-pot synthesis and post-synthetic modification of nanomofs using droplet nanoreactors. *Scientific reports*, 6(1):1–9, 2016.

[42] Sujay Bagi, Shuai Yuan, Sergio Rojas-Buzo, Yang Shao-Horn, and Yuriy Román-Leshkov. A continuous flow chemistry approach for the ultrafast and low-cost synthesis of mof-808. *Green Chemistry*, 23(24):9982–9991, 2021.

[43] Lei Zhang and Younan Xia. Scaling up the production of colloidal nanocrystals: should we increase or decrease the reaction volume? *Advanced materials*, 26(16):2600–2606, 2014.

[44] Carlos Echaide-Górriz, Coralie Clément, Fernando Cacho-Bailo, Carlos Téllez, and Joaquín Coronas. New strategies based on microfluidics for the synthesis of metal–organic frameworks and their membranes. *Journal of Materials Chemistry A*, 6(14):5485–5506, 2018.

[45] Sujay D Bagi, Allan S Myerson, and Yuriy Román-Leshkov. Solvothermal crystallization kinetics and control of crystal size distribution of mof-808 in a continuous flow reactor. *Crystal Growth & Design*, 21(11):6529–6536, 2021.

[46] Mathieu Gonidec and Josep Puigmartí-Luis. Continuous-versus segmented-flow microfluidic synthesis in materials science. *Crystals*, 9(1):12, 2019.

[47] Pablo Martinez-Bulit, Alessandro Sorrenti, David Rodriguez-San-Miguel, Michele Mattera, Yonca Belce, Yanming Xia, Shenglin Ma, Mu-Hua Huang, Salvador Pané, and Josep Puigmartí-Luis. In flow-based technologies: a new paradigm for the synthesis and processing of covalent-organic frameworks. *Chemical Engineering Journal*, page 135117, 2022.

[48] Jia Huo, Mark Brightwell, Samir El Hankari, Ashesh Garai, and Darren Bradshaw. A versatile, industrially relevant, aqueous room temperature synthesis of hkust-1 with high space-time yield. *Journal of Materials Chemistry A*, 1(48):15220–15223, 2013.

[49] Jesse LC Rowsell and Omar M Yaghi. Effects of functionalization, catenation, and variation of the metal oxide and organic linking units on the low-pressure hydrogen adsorption properties of metal- organic frameworks. *Journal of the American Chemical Society*, 128(4):1304–1315, 2006.

[50] Ashlee J Howarth, Aaron W Peters, Nicolaas A Vermeulen, Timothy C Wang, Joseph T Hupp, and Omar K Farha. Best practices for the synthesis, activation, and characterization of metal–organic frameworks. *Chemistry of Materials*, 29(1):26–39, 2017.

[51] Checkers R Marshall, Emma E Timmel, Sara A Staudhammer, and Carl K Brozek. Experimental evidence for a general model of modulated mof nanoparticle growth. *Chemical science*, 11(42):11539–11547, 2020.

[52] Franck Millange, Manuela I Medina, Nathalie Guillou, Gérard Férey, Kathryn M Golden, and Richard I Walton. Time-resolved in situ diffraction study of the solvothermal crystallization of some prototypical metal–organic frameworks. *Angewandte Chemie*, 122(4):775–778, 2010.

[53] Franck Millange, Racha El Osta, Manuela E Medina, and Richard I Walton. A time-resolved diffraction study of a window of stability in the synthesis of a copper carboxylate metal–organic framework. *CrystEngComm*, 13(1):103–108, 2011.

[54] Rijia Lin, Lei Ge, Hui Diao, Victor Rudolph, and Zhonghua Zhu. Ionic liquids as the mofs/polymer interfacial binder for efficient membrane separation. *ACS applied materials & interfaces*, 8(46):32041–32049, 2016.

[55] Camille Petit and Teresa J Bandosz. Exploring the coordination chemistry of mof–graphite oxide composites and their applications as adsorbents. *Dalton Transactions*, 41(14):4027–4035, 2012.

[56] Xuejiao Sun, Xiulian Gu, Wentao Xu, Wen-Jie Chen, Qibin Xia, Xiaoyang Pan, Xiaojing Zhao, Yi Li, and Qi-Hui Wu. Novel hierarchical fe (iii)-doped cu-mofs with enhanced adsorption of benzene vapor. *Frontiers in chemistry*, page 652, 2019.

[57] G Mahalakshmi and V Balachandran. Ft-ir and ft-raman spectra, normal coordinate analysis and ab initio computations of trimesic acid. *Spectrochimica Acta Part A: Molecular and Biomolecular Spectroscopy*, 124:535–547, 2014.

[58] Aparna Shastri, Asim Kumar Das, Sunanda Krishnakumar, Param Jeet Singh, and BN Raja Sekhar. Spectroscopy of n, n-dimethylformamide in the vuv and ir regions: Experimental and computational studies. *The Journal of Chemical Physics*, 147(22):224305, 2017.

[59] Enrica Biemmi, Sandra Christian, Norbert Stock, and Thomas Bein. High-throughput screening of synthesis parameters in the formation of the metal-organic frameworks mof-5 and hkust-1. *Microporous and Mesoporous Materials*, 117(1-2):111–117, 2009.

[60] Copper benzene-1,3,5-tricarboxylate (basolite c300; cu-btc mof; hkust-1, purchased commercial material (lot stbc4614 v)), cu_3 $((o_2\ c)_3c_6h_3)_2$. sample was dehydrated at 423 k overnight under vaccum. pattern measured at beam line 11-bm, (goniometer radius 1000 mm) advanced photon source, argonne national laboratory, lement illinois, usa. data collected using debye-scherred geometry. kaduk, j. polycrystallography inc., naperville, il, usa.

[61] Kenneth SW Sing and Ruth T Williams. Physisorption hysteresis loops and the characterization of nanoporous materials. *Adsorption Science & Technology*, 22(10):773–782, 2004.

[62] Timothy Steenhaut, Nicolas Grégoire, Gabriella Barozzino-Consiglio, Yaroslav Filinchuk, and Sophie Hermans. Mechanochemical defect engineering of hkust-1 and impact of the resulting defects on carbon dioxide sorption and catalytic cyclopropanation. *RSC Advances*, 10(34):19822–19831, 2020.

[63] Andrea Domán, Janos Madarász, György Sáfrán, Ying Wang, and Krisztina László. Copper benzene-1, 3, 5-tricarboxylate (hkust-1)–graphene oxide pellets for methane adsorption. *Microporous and Mesoporous Materials*, 316:110948, 2021.

[64] Alan Ranodolph. *Theory of particulate processes: analysis and techniques of continuous crystallization*. Elsevier, 2012.

[65] Helen Song, Michelle R Bringer, Joshua D Tice, Cory J Gerdts, and Rustem F Ismagilov. Experimental test of scaling of mixing by chaotic advection in droplets moving through microfluidic channels. *Applied physics letters*, 83(22):4664–4666, 2003.

[66] Helen Song, Delai L Chen, and Rustem F Ismagilov. Reactions in droplets in microfluidic channels. *Angewandte chemie international edition*, 45(44):7336–7356, 2006.